Anal Bioanal Chem (2012) 402:2511–2519
DOI 10.1007/s00216-011-5194-x

ORIGINAL PAPER

What determines MALDI ion yields? A molecular dynamics study of ion loss mechanisms

Richard Knochenmuss · Leonid V. Zhigilei

Received: 6 April 2011 / Revised: 25 May 2011 / Accepted: 19 June 2011 / Published online: 3 July 2011

Abstract Ion recombination in matrix-assisted laser desorption/ionization (MALDI) is as important as any ion formation process in determining the quantity of ions observed but has received comparatively little attention. Molecular dynamics simulations are used here to investigate some models for recombination, including a Langevin-type model, a soft threshold model and a tunneling model. The latter was found to be superior due to its foundations in a widespread physical phenomenon, and its lack of excessive sensitivity to parameter choice. Tunneling recombination in the Marcus inverted region may be a major reason why MALDI is a viable analytical method, by allowing ion formation to exceed ion loss on the time scale of the plume expansion. Ion velocities, photoacoustic transients and pump-probe measurements might be used to investigate the role of recombination in different MALDI matrices, and to select new matrices.

Keywords MALDI ionisation · Recombination · Molecular dynamics

Published in the special issue *Analytical Sciences in Switzerland* with guest editors P. Dittrich, D. Günther, G. Hopfgartner, and R. Zenobi.

R. Knochenmuss (✉)
Tofwerk AG,
Uttigenstrasse 22,
3600 Thun, Switzerland
e-mail: rknochenmuss@gmx.net

L. V. Zhigilei
Department of Materials Science and Engineering,
University of Virginia,
395 McCormick Road,
Charlottesville, VA 22904-4745, USA

Introduction

Mechanistic understanding of matrix-assisted laser desorption/ionization (MALDI) is essential for efficient, rational development of this widely used analytical technique. Considerable progress has been made in recent years, see Ref. [1] for a recent review. The physical chemistry involved falls into several categories: (1) thermal and mechanical aspects such as heating, phase change, clustering, and plume expansion [2]; (2) photophysics and chemistry of the matrix leading to primary matrix ion formation; (3) primary ionization processes which do not involve matrix, such as direct analyte photoionization, or ionization during the sample preparation process ("preformed" ions); (4) secondary reactions of primary ions with neutrals during ablation, whether by electron transfer, proton transfer, or ion adduct formation; and (5) the loss mechanism of charge recombination. These components are obviously coupled, in many cases quite strongly.

Attention to date has focused largely on the first four components, especially the question of primary ion formation. This is natural, since a major objective is to maximize MALDI sensitivity by creating as many primary ions as possible, with consequent increased formation of secondary analyte ions. Many questions about MALDI ion formation remain inadequately answered, and only a few matrices have been investigated in any detail. However, even more questions remain regarding the other major factor limiting MALDI ion yield: loss mechanisms.

Ion yields in the 10^{-4} to 10^{-3} range have been reported [3–7]. Unless the primary ionization processes have similarly low efficiency, loss rates in MALDI must be high. Among other considerations, such as low typical charge states of large biomolecules, this led Karas et al. to describe ion recombination as the process which ions must

escape to become a "lucky survivor" in their 2000 model [8]. While important as a framework to plausibly explain aspects of observed spectra, that model does not make quantitative predictions, nor provide insight about recombination rates or mechanisms. It is also incompatible with some MALDI phenomena [1]. The initial model suggested a major role for free electrons, but it is now clear from electron capture cross sections [9–11] and binding energies [12] of matrix molecules that these are short-lived. Instead, matrix anions are the dominant negative charge carriers. For the same reasons, only a few-nanometer region at the surface of the sample will develop a net positive charge due to electron escape. In addition, any photoelectrons due to laser light reaching a metal sample substrate are more than compensated by enhanced matrix ionization at the interface [13, 14]. Later developments [15, 16] placed less emphasis on electrons and more on clusters, the model remained entirely qualitative. Reactions in clusters were also a central theme of several studies and proposals of the Tabet group [17–20].

Going beyond qualitative approaches, many MALDI phenomena have successfully been qualitatively or semi-quantitatively treated using a two-step model involving primary matrix ionization followed by secondary ion–molecule reactions with analytes [21–23]. The MALDI sample and ablation plume is treated as a reaction vessel, and differential rate equations for the various physical and chemical processes, including recombination, are numerically integrated to give the final ion populations that can be observed as a mass spectrum [21–23]. Most recently, this approach was successfully applied to question of positive versus negative ion ratios [23], where it was shown that these are the combined effect of thermodynamic limits in the individual polarities but kinetically limited interconversion reactions.

The importance of recombination in the two-step model is illustrated in Fig. 1. The maximum ion population is much higher than the final number of released ions. Most of the losses occur early, when ions become mobile following the phase transition, but the density is still high. Because density and pressure strongly influence loss rates, the phase transition is an important part of the model.

In the rate equation model, the sample is assumed to vaporize completely at a fixed temperature. Since rapid laser ablation processes like MALDI are unlikely to be so straightforward [24–32], a molecular dynamics implementation of the two-step model was developed, including the same photochemical processes but with far fewer restrictions on the physical evolution of the system [33, 34]. Recombination losses in the MD model are similar in magnitude to those of the rate equation results, as seen in Fig. 1.

While the success of the rate equation model strongly suggests that the parameters used are at least approximately correct, this begs the question of what determines these, and how they might be influenced. In molecular dynamics, reaction probabilities must be specified in more detail. At the least, some rate versus distance function must be included, which implicitly or explicitly represents particular physical processes. As already noted in the first MALDI molecular dynamics reports, the recombination model and parameters are among the most sensitive factors in the model [33]. The present work explores this aspect of MALDI in more detail.

Recombination in MALDI may involve a variety of species. Molecular radical ions are readily observed for many analytes in MALDI, and electron transfer reactions between them, and with matrix, have been investigated in detail [35–38]. However, more analytes are observed as proton adducts and/or as deprotonated anions. In addition, alkali metal adducts are commonly observed. As noted above, free electrons may be largely disregarded, in favor of matrix anions.

Reaction between molecular cations and anions will obviously be an electron transfer process. The net reaction between protonated and deprotonated species is proton transfer but may in fact proceed by electron transfer followed by hydrogen transfer. Proton tunneling is also known and might play some role in MALDI, but it is not expected to be significant. Being 1,836 times lighter than protons, electrons have a much larger tunneling range, which has a dependence like $\exp(-(\text{mass})^{1/2})$. As a result, it is highly probable that recombination of protonated/deprotonated species in MALDI will generally proceed by a sequential electron-hydrogen transfer, in which the electron transfer step is rate determining:

$$MH^+ + (M-H)^- \rightarrow MH^\circ + (M-H)^\circ \rightarrow 2M$$

Even if the hydrogen transfer (second) step is slow, neutralization by electron tunneling is the first step and the only step relevant for the present simulations.

In the rate equation model, neither the types of ions nor the mode of recombination need be specified. Based on the considerations above, the present molecular dynamics model assumes all ions to be of equivalent type, and that recombination to proceed by a single mechanism. In the two threshold models below, the ions and mechanism need not be further specified. In the tunneling model, all recombinations are assumed to occur by electron tunneling, with an implicit second neutral atom transfer, if one wishes to imagine the ions to be protonated/deprotonated molecules.

Computational methods

The breathing sphere molecular dynamics model has been described previously [24–28]. The extensions of the model

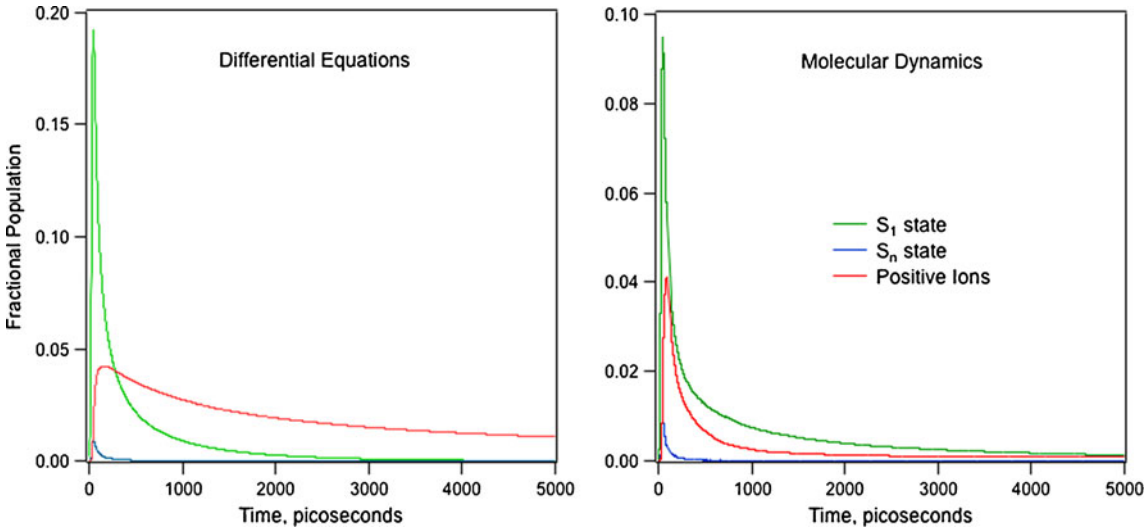

Fig. 1 Comparison of rate equation and molecular dynamics models of MALDI. In both models, ions are formed by pooling of the S_1 and S_n electronic excited states. When these are abundant ion formation is rapid, but then is followed by extensive recombination losses. The difference between formation and recombination at the end of the plume expansion represents the experimentally observable ion yield

to include the photophysics and ion–molecule chemistry of MALDI have been reported in refs [33, 34].

In this study, the simulated samples were smaller than in previous MALDI work, to enable rapid comparison of models and parameter sets. The dimensions were 72.5 by 10 by 10 nm, with 49,910 matrix molecules. In contrast to the earlier simulations, no pressure transmitting boundary conditions were applied at the back of the sample. Periodic boundary conditions were applied in the lateral directions, so the simulation corresponds to a free standing film. The sample is completely ablated at the laser fluences used.

The 355-nm Gaussian laser pulse had 35 ps temporal width. The parameters of the new recombination models will be described below. They apply to both matrix and analyte, but results for analyte are not presented here. Otherwise all intermolecular potentials and simulation parameters were as reported previously, with parameters appropriate for DHB matrix. The simulations were performed on a variety of personal computers, and required approximately 2 weeks to simulate one nanosecond of a MALDI event.

Recombination models and results

In the models to date, both electronic excitations (excitons) and charges have been assumed to be highly localized, but mobile. Exciton hopping and pooling (reaction of two excitons) are key processes in ion formation, and described using pairwise interactions. Charge is assumed to be fully localized on individual molecules. (Note that the molecular dynamics technique used is molecular rather than atomistic, so localization within the molecule is not possible.) Charge is also mobile, in that it is allowed to hop from one molecule to another, if this hop reduces the total energy of the system.

As the temperature increases, the material is vaporized, which may be an explosive event, if fast energy deposition leads to strong overheating. During this period, and in the later expansion, all species are increasingly translationally mobile, mean free paths increase quickly, and electrostatic screening decreases with density. Due to the long-range nature of the Coulomb force, oppositely charged species are then attracted over long distances. MALDI becomes a race between recombination and separation of charges by the plume expansion. Charge separation may be aided by applied external fields but only after ion motion is dominated by those fields and not by collisions.

Hard threshold

The recombination picture used up to now is essentially equivalent to the Langevin model of solid-state physics [39]. The rate is limited by how fast ions find each other. At a threshold radius, recombination is taken to occur effectively instantaneously, being much faster than charge motion. In the MD model, charge moves either by molecular translational motion, or by hopping. A hop is allowed if the total energy of the system is, thereby, decreased. The energy decrease can come either from a more favorable total charge distribution, if the charge is transferred between two like molecules, or by transfer of charge to a molecule with a higher affinity for that charge. This can be the case if transfer is to or from analytes, which have different proton or electron affinities than the matrix.

A hard threshold is intuitively attractive in cases where charge density and ion mobility are low, but it introduces the somewhat arbitrary recombination radius. This was found to be a very sensitive parameter in the original MALDI MD study [33]. The sensitivity comes not least from the fact that charge densities in simulated MALDI events are very high, as shown in Fig. 1, reaching several percent (depending on laser fluence). Note that in the case of face centered cubic packing of the model matrix, 1/12= 8.3 mol% would represent an average of about one nearest neighbor ion for every neutral. Diffusion or migration of charge is then not rate limiting during this part of the MALDI event. As a result, by choice of the recombination radius the fraction of ions surviving the ablation event can be varied from very high to very low values. This is largely a function of the typical closest approach distances at the highest temperatures reached, and therefore a function of the intermolecular potentials used.

Soft threshold

Since charge migration is not the limiting factor during an important, if short, part of the MALDI event, the approach needs to be revised. It is physically more reasonable to use a model in which the probability of recombination increases smoothly with distance. An obvious first step away from the hard threshold, but which retains an agnostic view of the underlying mechanism, is to use a soft threshold. The logistic function was tested for this, which has the form:

$$P(R) = 1 - 1/(1 + \exp(-(R - R_0)/W))$$

Where P is the probability of recombination between two oppositely charged ions at distance R. R_0 is the threshold distance, and W the width parameter. This function provides a smooth transition between unit and zero probability and is symmetric about R_0. It is shown for a range of width parameters in Fig. 2. The central value, R_0=1.675 Å, is in the range of the matrix–matrix closest approach distance, under typical simulated temperatures and pressures.

While this function does not imply or impose any particular mechanistic model, it does add a second parameter which must be empirically adjusted without physical guidance. The results must be evaluated by how the parameters influence the evolution of charge density during the event and the resulting net ion yield after significant plume expansion. It was found that as for the hard threshold, small changes in the parameters have a very large effect, particularly the radius. This sensitivity, coupled with the lack of a physical foundation, led to the conclusion that the soft threshold model is not significantly better than the hard threshold.

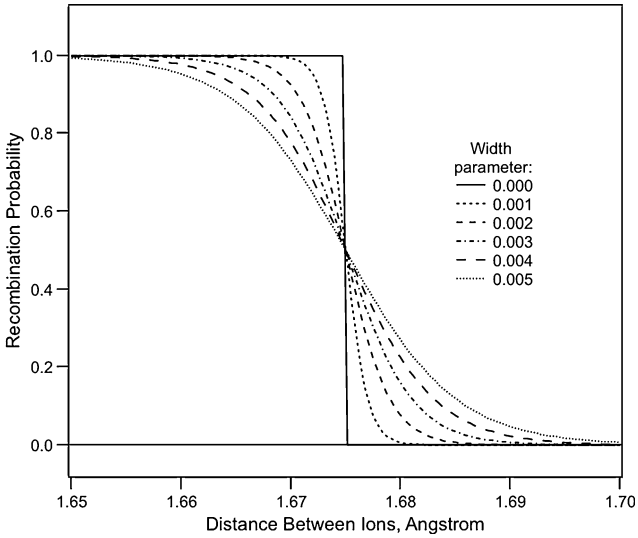

Fig. 2 Soft recombination threshold model, as represented by a logistic function

Tunneling

The threshold models require that the ions "touch," although the soft model assumes that the "edges" are slightly fuzzy. Molecules do not have sharp boundaries, and molecular electronic wavefunctions decay exponentially with distance, to a first approximation. As a result, molecules can "feel" each other, although weakly, at rather long distances. This is the basis for most treatments of electron tunneling, in a variety of settings. These include field electron emission, metal-insulator-metal junctions, scanning tunneling microscopy, and donor–acceptor molecular pairs, ranging from small molecules to ones as large as proteins.

In the golden rule of perturbative formulation, the tunneling probability is determined by the overlap of the donor and acceptor wavefunctions across the barrier created by the gap between them [40–42]:

$$P = K|< \psi_D| H_{\text{barrier}}|\psi_A >|^2$$

In the usual semiclassical Jeffreys, Wentzel, Kramers, Brillouin approach, the electronic wavefunctions decay exponentially inside a flat-top rectangular barrier. Their product, therefore, has an exponential dependence on the barrier width. The probability takes the form

$$P = K_0 \exp(-\beta R)|< \phi_D|\phi_A >|^2$$

Where K_0 corresponds to the maximum probability at zero effective barrier width, β describes the decay of electronic overlap with barrier width R, and the matrix element $\langle \phi_D | \phi_A \rangle$ is over the vibrational part of the wavefunctions, usually known as the Franck–Condon factor.

Since the molecular geometry may undergo significant changes as electrons are added to or removed from bonding and nonbonding orbitals, the vibrational potential surfaces relevant for the Franck–Condon factors are typically substantially displaced in some internal coordinates. Tunneling rates may then depend on the relative vertical displacement of the surfaces, which changes the wavefunction overlap. This displacement is closely related to the net energy difference of the donor and acceptor states, the ΔG of the reaction. It can go through a maximum at some ΔG and decrease at yet more negative ΔG. This is known as the Marcus inverted region.

Including the zero barrier maximum rate, α, the exponential intermolecular distance exponent, β, and the Franck–Condon factor, a general expression for tunneling rate per second is [43–45]:

$$\log_{10}(k) = \alpha - \beta R - K_v(\Delta G + \lambda)^2/\lambda$$

Where the vibrational surface overlap has been expressed in terms of the reaction free energy and a reorganizational energy, λ, with a scale factor for the Franck–Condon factor of K_v. This expression is valid for a flat-top barrier, which is physically correct if there is no potential difference across the barrier. Since we are explicitly interested in the case where opposite charges approach, there is an electric field in the barrier region. In addition, external fields may be applied during the ablation event. A tilted barrier potential can be treated [46], but is not included here, since it adds further complications which may not be warranted, in view of the simplicity of the overall approach.

Measurements are lacking on electron tunneling rates in MALDI matrix materials. In the absence of contrary evidence, they will be treated here as typical organic substances. Considerable effort has been expended in investigating electron tunneling reactions since they are both fundamental to life, and relevant to industrial electrochemistry. Typical values for α and β for many donor–acceptor pairs, both small and large, are 13 and 0.5–1.1, respectively [43, 47]. The α parameter corresponds to a typical frequency factor in reaction rate theory, while the decay exponent β depends on the height of the barrier. In molecular terms, β often corresponds roughly to the $\sigma \rightarrow \sigma^*$ energy and, therefore, is rather generic for most organic materials. Based on these considerations, these widely applicable values of α and β are considered likely to be reasonable for MALDI materials as well.

The reorganizational energy, λ, is more problematic. It depends on the specific nature of the donor and acceptor molecules and their potential surfaces. Electron transfer between otherwise uncharged donor and acceptor sites in proteins must take place on a qualitatively different surface than transfer between positively and negatively charged molecules in MALDI. Without further information, it was considered best to avoid unreliable estimates of this parameter, and it was not explicitly included in the calculations. This is not considered a significant limitation, since this term is not dependent on intermolecular distance, and therefore has the same effect as reducing α. For this reason some calculations using α=12, as well as α=13, were performed.

The only significant loss of generality in omitting this term is that it includes the temperature dependence. However, recombination involves a large negative-free energy change, which normally makes thermal activation relatively unimportant. It was considered more important to limit the unknown parameters to two, than to include a weak temperature dependence and two more, poorly known, parameters.

Figure 3 shows the time evolution of ion populations for α=13 and two β values. As is apparent, the barrier decay exponent has a large influence on the shape and height of the curves. A large exponent corresponds to reduced overlap of donor and acceptor wavefunctions, and a reduced recombination rate. As a result, the peak ion populations varied by about a factor of 1.67 between the extreme values of β tested here. This is very close to the corresponding ratio of wavefunction overlaps in the tunneling barrier, $\exp(-0.5)/\exp(-1.0) = 1.64$.

Following the peak, the β-dependent differences were even more pronounced, because recombination has a large effect on the rate of conversion of laser energy to heat. Considerable energy is initially stored in separated charges; fast recombination makes this available earlier than slow recombination. The consequence is a large difference in rate of ablation and expansion. In Fig. 3, the β=0.5 plot is already flat at a few 100 s of picoseconds because the film has explosively disintegrated and the remaining ions are entrained in a rapidly expanding gas. By contrast, the β=1.0 plot shows much more gradual heat conversion and consequent expansion. This is also apparent in Fig. 4, which shows the recombination rate versus time for the two simulations of Fig. 3.

The evolution of sample density which is associated with these differences is shown in the next figure. The dynamics of ablation are obviously quite different for slow and fast recombination. Rapid energy deposition not only led to earlier expansion, but also to higher velocities and less cluster formation. Secondary matrix-analyte ion–molecule reactions will be strongly modulated by such changes since they depend on the number of intermolecular collisions during the expansion [8, 23]. The number of analyte ions which are detected also depends on how many remain in clusters, and hence cannot appear at the correct mass/charge value.

As can be inferred from Fig. 5, the peak pressure reached was higher for fast recombination, since higher peak pressure

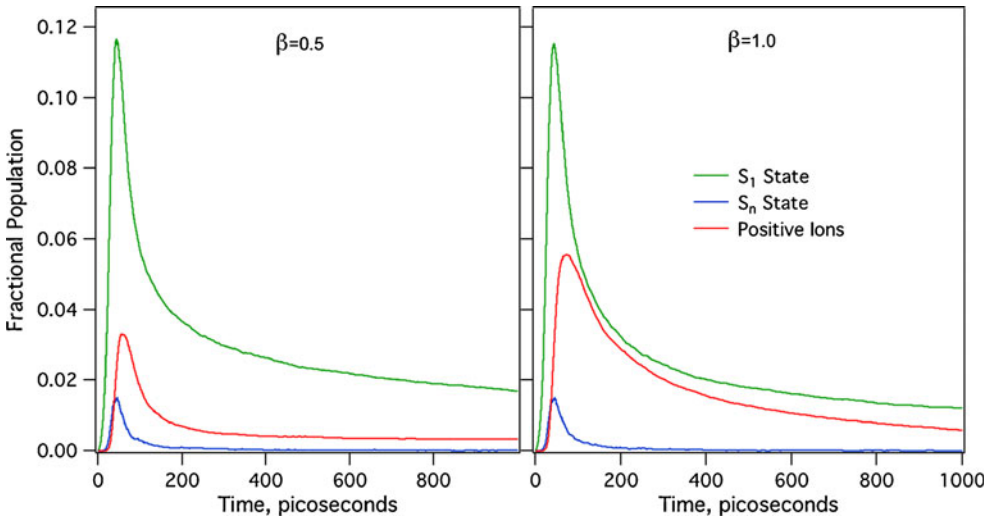

Fig. 3 Fractional excited state and positive ion populations versus time, calculated using the molecular dynamics model for α=13 and β=0.5 or 1.0. The laser pulse energy was 50 mJ/cm^2

leads to earlier and faster expansion. This scaled strongly, inversely and linearly with β (from about 275 to 50 MPa) if disintegration happened within about 150 ps after the laser pulse. Slower disintegration allowed the material to relax before much vapor formed, so the peak pressure was approximately the same (50 MPa) for all slow recombination rates. Similar trends were observed for different α. Higher α, and faster recombination, led to higher pressures.

The model parameters had a more modest effect on temperatures. The peak values were around 1,200 K in all cases. The peak temperature was reached early in simulations with fast recombination, and later for slow recombination. The slower effective heating in the latter cases allows for a more gradual expansion of the film and the corresponding decrease in the peak pressure. Note that in all simulations the peak temperature exceeds the threshold temperature for the onset of the explosive boiling of the overheated matrix represented by the breathing sphere model (1,060 K as determined in Ref. [28]). As a result, in all simulations shown in Fig. 5, an explosive disintegration of the irradiated film into a mixture of liquid droplets and vapor phase matrix molecules is observed.

A summary of peak and final (1 ns) ion populations is shown in Fig. 6. The peak climbs smoothly with β, and shows a parallel vertical shift with α. This smooth and systematic behavior is preferable to the high parameter sensitivity of the hard and soft thresholds. Among other advantages, it means that choice of parameters is much less critical, and tolerant of some error.

The ion populations at 1 ns are, of course, much lower. For α=13, all samples disintegrated relatively quickly, the 1 ns populations follow a smooth curve versus β. The difference between minimum and maximum is nearly a factor of two, more than for the peak populations. For α=12, and large β, disintegration was slow, and the density had not decreased much at 1 ns. Therefore, this curve shows two regions: a slowly varying part at low β, consistent with the α=13 results, a steeply rising part at high β. It is expected that this part of the α=12 curve will approach that of α=13 upon further expansion of the plume.

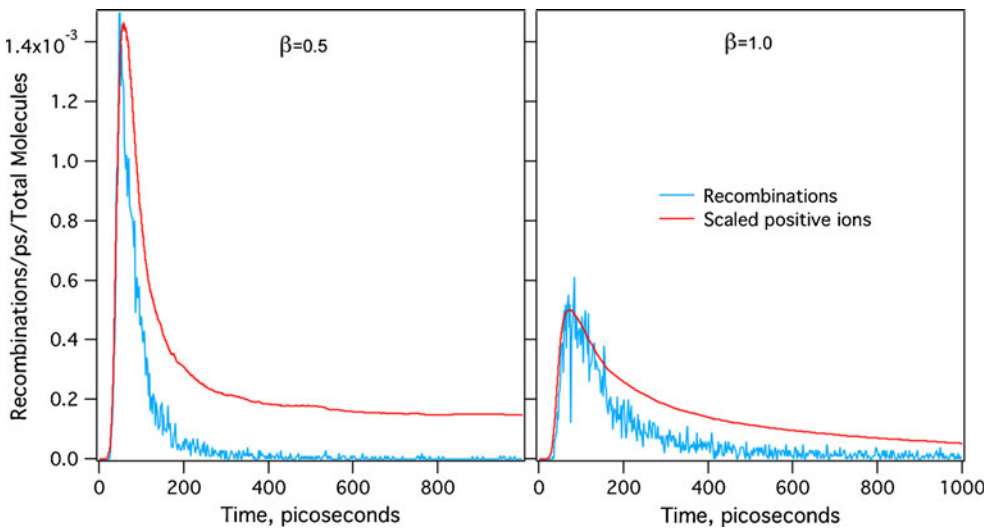

Fig. 4 Recombination rate for the simulations of Fig. 3. Also shown is the positive ion population, scaled to match the height of the recombination rate curve. During the high density period, the recombination rate scales with the ion density. As the expansion begins, the rate drops quickly. Both the peak rate and the decrease after the peak are greater for β=0.5 than for β=1.0

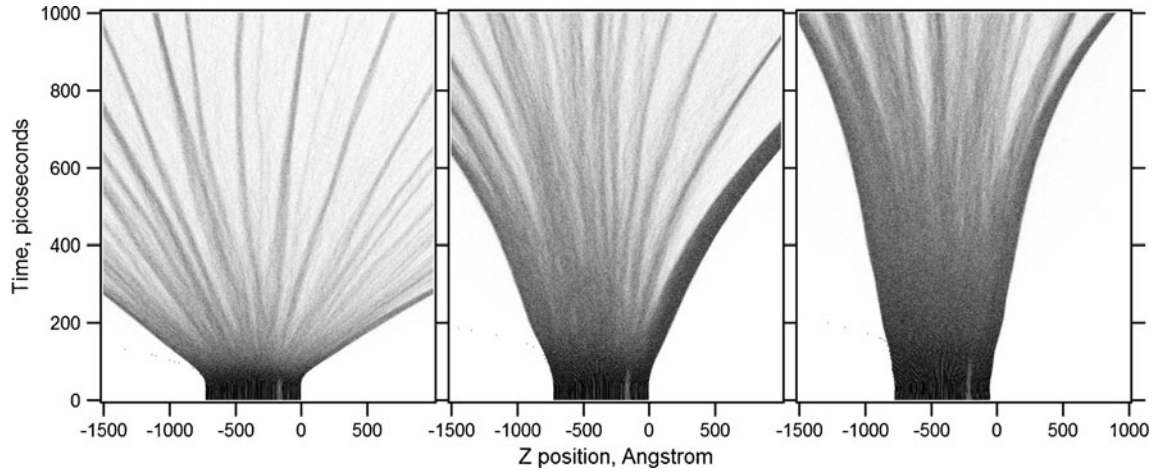

Fig. 5 Density versus time and axial position, for different recombination parameters. The laser was incident from the right onto the surface at Z=0, and the fluence was 50 mJ/cm^2. The tunneling parameters were, from left to right: α=13, β=0.5; α=13, β=1.0; and α=12, β=0.8. Darker regions are denser; the scale ranges from zero (*white*) to 770 molecules per nanometer in the Z direction (*black*)

Since the population of positive ions at any fixed time, such as 1 ns, depends on the sample density, which changes at a different rate in each simulation, an attempt was made to take this into account. Using the average density at the center of the sample, and the t=1 ns density of the α=13, β=1.0 simulation as the reference, the β dependence of Fig. 7 was obtained. The result is not qualitatively different from those at fixed times; there is a moderate increase in population for higher β.

Conclusions

Charge recombination is known to be as important as ion formation mechanisms in determining the analytical ion yield, but has been insufficiently investigated. In a first step, some models were compared using molecular dynamics simulations.

A simple model for recombination, in which charge diffusion to a contact radius is assumed to be rate determining, is very sensitive to parameters which cannot be readily linked to physical foundations. The charge density during important periods of the MALDI event is also too high for charge migration to be rate limiting, at least after the sample becomes fluid.

In contrast, electron tunneling is a common physical process when potential donors and acceptors are in near contact, making it a logical addition to the molecular dynamics MALDI model. Electron tunneling is considered to be a likely mechanism in all MALDI experiments, even if ions are primarily created by adduct formation, because electron tunneling does not require contact for charge transfer. In that case, adduct atom transfer presumably accompanies or follows the electron transfer.

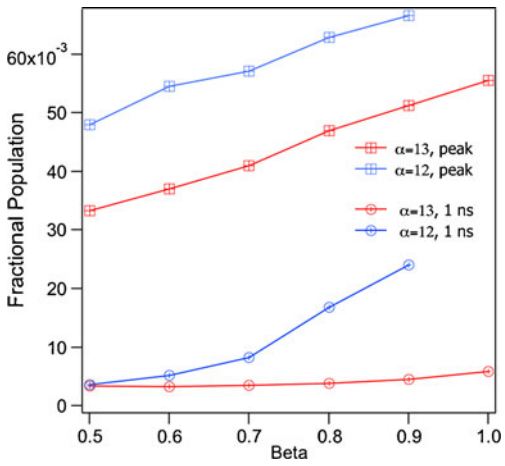

Fig. 6 Fractional-positive ion populations calculated using the molecular dynamics model, with α=13 and various values of β. Both the maximum value and the value at t=1 ns are shown. The laser fluence was 50 mJ/cm^2

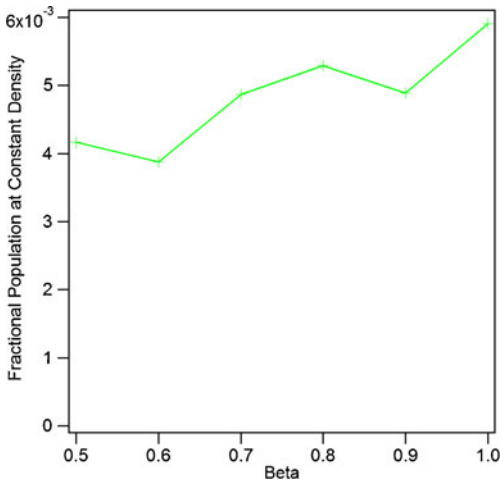

Fig. 7 Fractional-positive ion population as a function of β, for α=13, and laser fluence=50 mJ/cm^2, at similar central densities

In the absence of relevant tunneling information on MALDI matrix materials, parameters in the ranges found for numerous organic and biomolecules were tested. These parameter ranges led to physically plausible results that are consistent with experiment, and not overly sensitive to the exact parameter values.

MALDI recombination tunneling is certainly somewhere in the Marcus inverted region. Inverted region recombination in the solid state can become so unfavorable that the time scale stretches to hours [48], though this would not be possible in the fluid MALDI plume. This may be a major reason why MALDI is viable as an analytical method, allowing ion formation to exceed ion loss on the time scale of the plume expansion.

Pushing MALDI further into the inverted region would be desirable to enhance analytical performance. Most easily adjustable experimental parameters have little direct effect on the intermolecular interactions (short-range wavefunction overlap) which determine tunneling rates and ranges. Laser pulse energy, pulse width, extraction field or sample mixing ratio, for example, all have at best an indirect effect. But they do change the plume temperature, its rate of expansion, and reactant concentrations, which then influence ion–ion reaction rates. But specific tuning for low recombination without also affecting ion formation is not possible with these parameters.

More promising may be to optimize or select matrix materials with recombination in mind. Obviously, properties of the matrix affecting primary ion formation and secondary matrix-analyte reaction efficiencies must not be forgotten (such as proton affinity, ionization potential, absorption spectrum and ability to incorporate analytes into the crystal), but other matrix characteristics may contribute to MALDI performance by modulating recombination. For example, the electronic overlap factor will depend on how much and where charge is localized in donor and acceptor. If intersystem crossing is significant in donor or acceptor, as may be induced by heavy atoms such as halides (e.g., salts), triplet states may become important. In the denser period of MALDI ablation, multibody interactions will modulate the electronic states significantly, as is already observed in the form of exciton migration and pooling. If donor and acceptor form hydrogen bonded complexes, specific intermolecular orientations will be preferred, which may limit or enhance tunneling.

Selecting and optimizing for recombination also requires some experimental means of evaluating this aspect of MALDI performance. The recombination-induced heat pulse may provide a useful measure of how matrices differ in their recombination behavior. Photoacoustic studies of MALDI samples have been shown to be feasible [49]. The fivefold change found here in the peak pressure as a function of β suggests this might be a sensitive indicator, after correction for differences in matrix absorption cross sections. The heat pulse is also closely linked to the initial plume expansion velocity, so existing velocity data and generalizations about matrices as being "hot" or "cold" may be more a result of recombination efficiency than anything else.

Pump-probe experiments could also be used to gain further insight. These have also been carried out on MALDI samples, using lasers with similar pulse widths to those modeled here [50, 51]. The dependence of the ion yield for DHB matrix on delay between the pulses showed a distinct minimum at about 100 ps, followed by a broad maximum at about 2 ns. A reasonably similar form was calculated using the differential equation model [21] and attributed to the varying ionization efficiency of the second pulse in the early dense sample versus the less dense early plume. If true, this places a rather low time limit on the onset of sample disintegration. It would have to start no later than 100 ps after the initial laser pulse. This in turn suggests that, of the parameter sets tested here, high α (13) and low β (0.5–0.7) values are more likely to be correct, since they lead to faster and earlier ablation. Since the lower α value used, 12, was selected to roughly correspond to the case of a high vibrational reorganization energy, it seems unlikely that temperature is a large factor in MALDI tunneling.

Acknowledgment One of the authors (L. V. Z.) acknowledges financial support from the National Science Foundation (Award CMMI-0800786).

References

1. Knochenmuss R (2006) Ion formation mechanisms in UV-MALDI. Analyst 131:966–986
2. Dreisewerd K (2003) The desorption process in MALDI. Chem Rev 103:395–426
3. Puretzky AA, Geohegan DB (1997) Gas-phase diagnostics and LIF imaging of 3-hydroxypicolinic acid MALDI matrix plumes. Chem Phys Lett 286:425–432
4. Dreisewerd K, Schürenberg M, Karas M, Hillenkamp F (1995) Influence of the laser intensity and spot size on the desorption of molecules and ions in matrix-assisted laser-desorption/ionization with a uniform beam profile. Int J Mass Spectrom Ion Proc 141:127–148
5. Mowry C, Johnston M (1993) Simultaneous detection of ions and neutrals produced by matrix-assisted laser desorption. Rapid Comm Mass Spectrom 7:569–575
6. Quist AP, Huth-Fehre T, Sundqvist BUR (1994) Total yield measurements in matrix-assisted laser desorption using a quartz crystal microbalance. Rapid Commun Mass Spectrom 8:149–154
7. Ens W, Mao Y, Mayer F, Standing KG (1991) Properties of matrix-assisted laser desorption. Measurements with a time-to-digital converter. Rapid Commun Mass Spectrom 5:117–123
8. Karas M, Glückmann M, Schäfer J (2000) Ionization in MALDI: singly charged molecular ions are the lucky survivors. J Mass Spectrom 35:1–12
9. Pshenichnyuk SA, Asfandiarov NL (2004) The role of free electrons in MALDI: electron capture by molecules of alpha-cyano-4-hydroxycinnamic acid. Eur J Mass Spectrom 10:477–486

10. Pshenichnyuk SA, Asfandiarov NL, Fal'ko VS, Lukin VG (2003) Temperature dependence of dissociative electron attachment to molecules of gentisic acid, hydroquinone and *p*-benzoquinone. Int J Mass Spectrom 227:281–288
11. Pshenichnyuk SA, Asfandiarov NL, Fal'ko VS, Lukin VG (2003) Temperature dependencies of negative ion formation by capture of low-energy electrons for some typical MALDI matrices. Int J Mass Spectrom 227:259–272
12. Lippa TP, Eustis SN, Wang D, Bowen KH (2007) Electrophilic properties of common MALDI matrix molecules. Int J Mass Spectrom. submitted
13. Knochenmuss R, McCombie G, Faderl M (2006) The dependence of MALDI ion yield on metal substrates: photoelectrons from the metal vs. surface-enhanced matrix photoionization. J Phys Chem A 110:12728–12733
14. McCombie G, Knochenmuss R (2006) Enhanced MALDI ionization efficiency at the metal-matrix interface: practical and mechanistic consequences of sample thickness and preparation method. J Am Soc Mass Spectrom 17:737–745
15. Karas M, Krueger R (2003) Ion formation in MALDI: the cluster ionization mechanism. Chem Rev 103:427–439
16. Jaskolla TW, Karas M (2011) Compelling evidence for lucky survivor and gas phase protonation: the unified MALDI analyte protonation mechanism. J Am Soc Mass Spectrom 22:976–988
17. Alves S, Fournier I, Afonso C, Wind F, Tabet J-C (2006) Gas-phase ionization/desolvation processes and their effect on protein charge state distributions under MALDI conditions. Eur J Mass Spectrom 12:369–383
18. Fournier I, Brunot A, Tabet J-C, Bolbach G (2002) Delayed extraction experiments using a repulsive potential before ion extraction: evidence of clusters as ion precursors in UV-MALDI. Part I: dynamical effects with the matrix 2,5-dihydroxybenzoic acid. Int J Mass Spectrom 213:203–215
19. Fournier I, Brunot A, Tabet J-C, Bolbach G (2005) Delayed extraction experiments using a repulsive potential before ion extraction: evidence of non-covalent clusters as ion precursors in UV MALDI. Part II—dynamic effects with alpha-cyano-4-hydroxycinnamic acid matrix. J Mass Spectrom 40:50–59
20. Livadaris V, Blais J-C, Tabet J-C (2000) Formation of non-specfic protein cluster ions in MALDI: abundances and dynamical aspects. Eur J Mass Spectrom 6:409–413
21. Knochenmuss R (2002) A quantitative model of ultraviolet matrix-assisted laser desorption and ionization. J Mass Spectrom 37:867–877
22. Knochenmuss R (2003) A quantitative model of UV-MALDI including analyte ion generation. Anal Chem 75:2199
23. Knochenmuss R (2009) A bipolar rate equation model of MALDI primary and secondary ionization processes, with application to positive/negative analyte ion rations and suppression effects. Int J Mass Spectrom 285:105–113
24. Zhigilei LV, Kodali PBS, Garrison BJ (1997) Molecular dynamics model for laser ablation and desorption of organic solids. J Phys Chem B 101:2028–2037
25. Zhigilei LV, Garrison BJ (2000) Microscopic mechanism of laser ablation of organic solids in the thermal stress confinement irradiation regime. J Appl Phys 88:1–18
26. Zhigilei LV (2003) Dynamics of the plume formation and parameters of the ejected clusters in short-pulse ablation. Appl Phys A 76:339–350
27. Zhigilei LV, Leveugle E, Garrison BJ, Yingling YG, Zeifman MI (2003) Computer simulations of laser ablation of molecular substrates. Chem Rev 103:321–348
28. Leveugle E, Zhigilei LV (2007) Molecular dynamics simulation study of the ejection and transport of polymer molecules in matrix-assisted pulsed laser evaporation. J Appl Phys 102:074914
29. Balazs L, Gijbels R, Vertes A (1991) Expansion of laser-generated plumes near the plasma ignition threshold. Anal Chem 63:314–320
30. Bencsura A, Navale V, Sadeghi M, Vertes A (1997) Matrix-guest energy transfer in matrix-assisted laser desorption. Rapid Commun Mass Spectrom 11:679–682
31. Kristyan S, Bencsura A, Vertes A (2002) Modeling the cluster formation during infrared and ultraviolet MALDI o foligonucleotides in succinic acid matrix with molecular mechanics. Theor Chem Acc 107:319–325
32. Wu X, Sadeghi M, Vertes A (1998) Molecular dynamics of matrix-assisted laser desorption of leucine enkephalin guest molecules from nicotinic acid host crystal. J Phys Chem B 102:4770–4778
33. Knochenmuss R, Zhigilei LV (2005) A molecular dynamics model of UV-MALDI including ionization processes. J Phys Chem B 109:22947–229957
34. Knochenmuss R, Zhigilei LV (2010) Molecular dynamics simulations of MALDI: laser fluence and pulse width dependence of plume characteristics and consequences for matrix and analyte ionization. J Mass Spectrom 45:333–346
35. Macha SF, McCarley TD, Limbach PA (1999) Influence of ionization energy on charge-transfer ionization in matrix-assisted laser desorption/ionization mass spectrometry. Anal Chim Acta 397:235–245
36. McCarley TD, McCarley RL, Limbach PA (1998) Electron-transfer ionization in matrix-assisted laser desorption/ionization mass spectrometry. Anal Chem 70:4376–4379
37. Streletskii A, Ioffe IN, Kotsiris SG, Barrow MP, Drewello T, Strauss SH, Boltalina OG (2005) In-plume thermodynamics of the MALDI generation of fullerene anions. J Phys Chem A 109:714–719
38. Hoteling AJ, Nichols WF, Giesen DJ, Lenhard JR, Knochenmuss R (2006) Electron transfer reactions in LDI and MALDI: factors influencing matrix and analyte ion intensities. Eur J Mass Spectrom 12:345–358
39. Langevin P (1903) Sur la loi de recombination des ions. Ann Chim Phys 28:433–530
40. Jortner J (1997) Spiers memorial lecture on dynamics. From isolated molecules to biomolecules. Faraday Discuss 108:1–22
41. Marcus RA (1997) Electron transfer reactions in chemistry. Theory and experiment. Pure Appl Chem 69:13–29
42. Marcus RA (1956) Marcus outer sphere electron transfer. J Chem Phys 24:966–978
43. Moser CC, Keske JM, Warncke K, Farid RS, Dutton PL (1992) Nature of biological electron transfer. Nature 355:796–802
44. Gray HB, Winkler JR (2005) Long-range electron transfer. Proc Nat Acad Sci U S A 102:3534–3539
45. Moser CC, Anderson JL, Dutton PL (2010) Guidelines for tunneling in enzymes. Biochim Biophys Acta 1797:1573–1586
46. Knochenmuss R (1986) Theory of inelastic electron tunneling intensities which includes a non-constant barrier potential. Phys Rev B 33:7998
47. Gray HB, Winkler JR (2009) Electron flow through proteins. Chem Phys Lett 483:1–9
48. Schultz NA, Scharber MC, Brabec CJ, Saricifitci NS (2001) Low-temperature recombination kinetics of photoexcited persistent charge carriers in conjugated polymer/fullerene composite films. Phys Rev B 64:245210–245217
49. Rohlfing A, Menzel C, Kukreja LM, Hillenkamp F, Dreisewerd K (2003) Photoacoustic analysis of MALDI processes with pulsed infrared lasers. J Phys Chem B 107:12275–12286
50. Knochenmuss R, Vertes A (2000) Time-delayed 2-pulse studies of MALDI matrix ionization mechanisms. J Phys Chem B 104:5406–5410
51. Moskovets E, Vertes A (2002) Fast dynamics of ionization in UV MALDI of biomolecules. J Phys Chem B 106:3301–3306